Catalysis Today 138 (2008) 266–271

Contents lists available at ScienceDirect

Catalysis Today

journal homepage: www.elsevier.com/locate/cattod

Hydrogen storage in $CeNi_XO_Y$ and $CeM_{0.5}Ni_XO_Y$ (M = Zr or Al) mixed oxides

L. Jalowiecki-Duhamel [a,*], S. Debeusscher [a], H. Zarrou [a], A. D'Huysser [a], H. Jobic [b], E. Payen [a]

[a] UCCS Unité de Catalyse et de Chimie du Solide, UMR CNRS 8181, Bât. C3, Université des Sciences et Technologies de Lille, 59655 Villeneuve d'Ascq Cedex, France
[b] IRCELYON, Institut de Recherche sur la Catalyse et l'Environnement de Lyon, 2 Avenue Albert Einstein, 69626 Villeurbanne Cedex, France

ARTICLE INFO

Article history:
Available online 27 August 2008

Keywords:
Hydrogen storage
Oxyhydride
Anionic vacancy
Nickel oxide
Ceria–zirconia

ABSTRACT

$CeM_ZNi_XO_Y$ mixed oxides (M = Zr or Al, $Z = 0$ or 0.5, $0 \leq X \leq 3$) are large catalytic hydrogen reservoirs, called oxyhydrides, once treated in H_2. A catalytic chemical reaction is used to reveal and titrate reactive hydrogen species present in the solid. Different physicochemical techniques including XPS, ion sputtering, XRD, TPR, TGA, and inelastic neutron scattering (INS) have been used to characterize the solids. Depending on the composition and metal loading, a solid solution and/or a highly dispersed nickel oxide in ceria (or ceria–zirconia) can be obtained. Ion sputtering followed by XPS analysis has been very useful for estimating the size of NiO clusters (≈10 Å) present in the compounds. INS shows the coexistence of different hydrogen species that can be related to hydride species, hydrogen species in interaction with metallic nickel, as well as hydrogen species from hydroxyl groups.

1. Introduction

The potential benefits of a hydrogen economy coming from renewable energy sources are creating a large consensus; however, these interesting perspectives depend on the development of critical and key technologies such as fuel cells and hydrogen storage. Many metals and alloys are able to reversibly absorb large amounts of hydrogen. Charging can be done using molecular hydrogen gas or hydrogen atoms from an electrolyte. Besides, the ability of a material to interact with hydrogen is important either for hydrogen storage or for fuel cells electrodes.

The reaction of catalysts with hydrogen is complex but of great importance when the catalytic reactions involve hydrogen transfers. Ni metal or noble metals are often used as catalytically active components. Many research groups have developed various Ni catalysts because of a high cost of noble metals. Catalytic activities are affected by surface and structural properties as well as dispersion and reducibility of catalysts. The nature of hydrogen is not clear and different species can be created and transported. In our laboratory, it has been shown that some materials presenting very good catalytic activities [1,2] such as mixed oxides are able to store high quantities of hydrogen [3–5]. Similarly $CeNi_5$ oxide reduced in H_2 could store as much hydrogen as $CeNi_5$ intermetallic compound [2,3]. Different physicochemical techniques have been used to characterize the processes occurring during the hydrogen treatment of the cerium and nickel-based mixed oxides [6]. $CeNi_XO_Y$ oxides can be described as a mixture of nickel oxide with ceria modified by the insertion of a part of nickel in its lattice (solid solution). The size of the nickel oxide varies considerably from clusters to a crystallized material, depending on the X value and the experimental conditions.

This work concerns the interaction of hydrogen with a series of $CeM_ZNi_XO_Y$ (M = Zr or Al, $Z = 0$ or 0.5, $0 \leq X \leq 3$) mixed oxides, as these solids appeared as being able to store high quantities of catalytic hydrogen [4,7]. Various physicochemical techniques are used to understand the ability of the partially reduced solids to store hydrogen and analyze the nature and localization of the occluded hydrogen species.

2. Experimental methods

NiO and the mixed oxides denoted $CeNi_XO_Y$, $CeAl_{0.5}Ni_XO_Y$ and $CeZr_{0.5}Ni_XO_Y$ where X is the Ni/Ce atomic ratio were prepared by coprecipitation of the corresponding hydroxides from mixtures of cerium, nickel and aluminium or zirconium nitrates (0.5 M) using triethylamine (TEA) as a precipitating agent. After filtration, the solids are dried at 100 °C and calcined in air at 500 °C for 4 h [7,8]. The loading was measured by microanalysis and the proportion of Ni in the solids is presented by the Ni/M_T atomic ratio with M_T = Ni + Ce + Zr.

X-ray powder diffraction (XRD) analysis was carried out with a Siemens D 5000 diffractometer using a copper target. The crystallite size was estimated using the Scherrer equation from the most intense reflections observed for the NiO and CeO_2 crystallographic structures (1 1 1), (2 0 0), and (2 2 0) [6].

* Corresponding author. Tel.: +33 3 20 33 77 35; fax: +33 3 20 33 65 61.
E-mail address: louise.duhamel@univ-lille1.fr (L. Jalowiecki-Duhamel).

0920-5861/$ – see front matter © 2008 Elsevier B.V. All rights reserved.
doi:10.1016/j.cattod.2008.06.031

X-ray photoelectron spectroscopy (XPS) spectra of the samples were obtained on a VG Escalab 220 XL instrument using Al Kα radiation ($h\nu$ = 1486.6 eV). Details of the spectrometer and experimental procedure are given in Ref. [9]. The anode was operated at a power of 300 W and the fixed retardation ratio (FRR) was applied. The base pressure attained during the analysis was 1.33×10^{-6} Pa. Ions sputtering conditions were carried out with an ionic energy of 2000 eV and an applied tension of 580 V.

Thermogravimetric (TGA) measurements were performed using a T.A. Instruments SDT 2960 equipped with a flow-gas system. The oxides were treated in a hydrogen flow (10% H_2, 2 l h^{-1}) and the temperature was increased at a rate of 1.7 °C min^{-1} from room temperature to the final temperature of about 700 °C.

Temperature-programmed reduction (TPR) was performed on a Micrometrics Autochem 2920 analyser, and hydrogen consumption was measured by a TCD detector: 25 mg of the sample was treated in 5% H_2–95% Ar gas mixture (2 l h^{-1}). The temperature was increased to 800 °C at a heating rate of 10 °C min^{-1}.

Measurement of the hydrogen stored in the solid is based on the ability of this class of compounds to hydrogenate 2-methylbut-1,3-diene (isoprene) in the absence of gaseous hydrogen [10]. The pretreatment and catalytic experiments were carried out in situ at atmospheric pressure. The solid was treated first (12 h) in a purified hydrogen flow at various temperatures T_T between 50 °C and 700 °C. Then, after elimination of molecular hydrogen, hydrogenation reaction was performed in isoprene + helium mixture. The hydrogenation reaction involves the participation of reactive hydrogen species of the solid (noted H*), which can diffuse from bulk to hydrogenate isoprene at the surface on a hydrogenation site.

Inelastic neutron scattering (INS) experiments were performed using the IN1 BeF spectrometer at ILL. 36 g of solid were placed inside stainless steel containers, and the different treatments (10 h) were performed using high purity gases. INS experiments were carried out at 10 K using the Cu (2 0 0) monochromator for energy transfers between 80 cm^{-1} and 380 cm^{-1} and the Cu (2 2 0) monochromator for energy transfers between 380 cm^{-1} and 3000 cm^{-1}. INS emphasizes motions of hydrogen species because the scattering cross-section is much higher for hydrogen (80 b) than for other elements (5 b).

3. Results and discussion

3.1. Synthesized mixed oxides properties

Some structural differences can exist in oxidized state of the mixed oxides, depending on various parameters such as precipitating agent or calcination temperature [2,6]. Therefore some XRD and XPS characterizations are necessary to analyze the obtained samples.

3.1.1. XRD

Only a ceria like phase is apparent in every solid analyzed (34-0394 JCPDS file) while crystallized NiO (4-0835 JCPDS file) appears for a specific value of X above 0.4 (Fig. 1). No phase related to the presence of Zr or Al was observed. As already reported in previous studies on $CeNi_XO_Y$ [9], a careful examination of patterns shows that the addition of nickel affects not only the broadness of the ceria peaks, but also their position, as presented in Fig. 2, attributed to the substitution of Ce^{4+} cations (0.9 Å) by Ni^{2+} cations (0.7 Å) inside CeO_2 lattice and interpreted by the formation of a cerium–nickel solid solution [6,9]. It is reported on binary mixed oxides that the highest proportion of solid solution is obtained for the $CeNi_{0.5}O_Y$ compound (Ni/M_T = 0.3). The results reported in Fig. 2 show clearly that the presence of Zr affects even more drastically

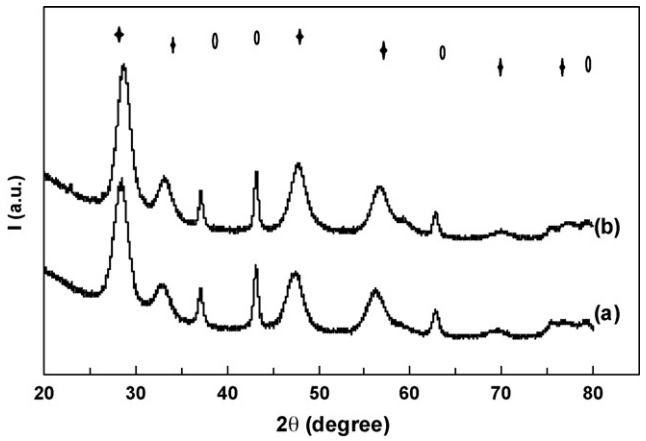

Fig. 1. XRD patterns of (a) $CeNi_1O_Y$ and (b) $CeZr_{0.5}Ni_1O_Y$ compounds. CeO_2 (✦) and NiO (○).

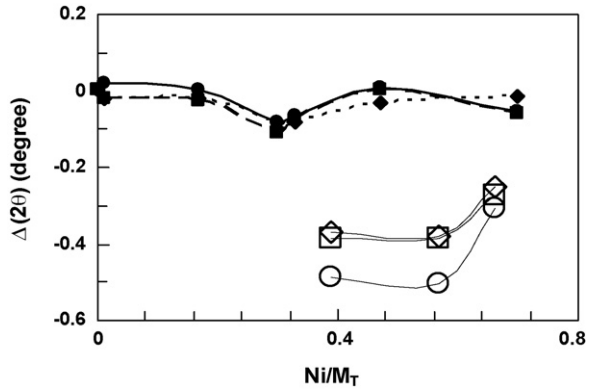

Fig. 2. Shift of CeO_2 diffraction peaks in $CeZr_{0.5}Ni_XO_Y$: (○) (1 1 1), (□) (2 0 0), (△) (2 2 0) and $CeNi_XO_Y$: (●) (1 1 1), (■) (2 0 0), (▲) (2 2 0). $\Delta(2\theta)$ = (peak position of reference oxide CeO_2) − (peak position of CeO_2-like phase in mixed oxide).

the ceria phase forming a well known solid solution allowed by the size of Zr^{4+} cations (0.84 Å). On Al containing compounds it was already shown that the presence of Al ameliorates NiO dispersion [9]. An estimation of the crystallites size at about 50 Å for CeO_2-like species and about 100 Å for NiO species is obtained (Table 1).

3.1.2. XPS and depth sputtering

As for $CeNi_XO_Y$ and $CeAl_{0.5}Ni_XO_Y$ solids already studied through this technique in the laboratory [9], the characteristics of Ce3d spectra of $CeZr_{0.5}Ni_XO_Y$ compounds, allows to unambiguously ascribing the 3d envelope to Ce^{4+} cations in CeO_2-like species. O1s lines and $Ni2p_{3/2}$ band shapes are in agreement with Ni^{2+} species mainly forming a solid solution with ceria and/or ceria–zirconia. For high Ni/Ce ratios several types of surface nickel seem to coexist, in agreement with XRD. Moreover, the evolution of superficial nickel composition versus bulk nickel content (microanalysis) is

Table 1
Surface area (BET) and crystallite size (calculated from Scherrer equation)

Catalyst	Ni/M_T[a]	SA (m^2 g^{-1})	d CeO_2 (Å)	d NiO (Å)
NiO	1	25	–	>200
CeO_2	0	89	97	–
$CeNi_1O_Y$	0.47	105	46	96
$CeZr_{0.5}Ni_1O_Y$	0.39	113	46	118
$CeAl_{0.5}Ni_1O_Y$	0.41	75	55	110

[a] From microanalysis.

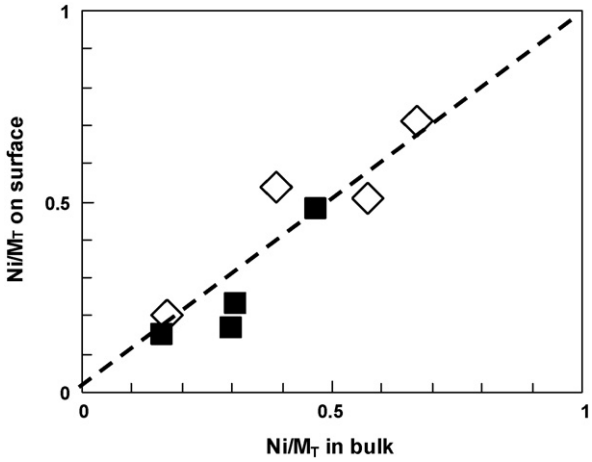

Fig. 3. Variation of Ni/M_T surface ratio (XPS) as a function of Ni/M_T bulk ratio (microanalysis) in $CeNi_XO_Y$ (■) and $CeZr_{0.5}Ni_XO_Y$ (◇) compounds.

Table 2
Estimation of NiO crystallites size by depth sputtering followed by XPS[a]

Solid solution	Particle size (Å)[a]	
	$CeZr_{0.5}Ni_1O_Y$	$CeNi_1O_Y$
Without	5	12
With	8	15

[a] Detailed and applied on similar compounds in Ref. [9].

close to the case of a homogeneous distribution of nickel inside the solid (45° diagonal line) (Fig. 3).

Ions sputtering in combination with surface analysis techniques such as XPS provide information on the in-depth distribution of elements inside the solid, and was previously detailed and applied in our laboratory to characterize some $CeNi_XO_Y$ compounds [9]. During the first minutes of sputtering there is a decrease of Ni/Ce ratio, confirming the structure does not correspond to a homogeneous solid solution. The presence of small crystallites in strong interaction with some bigger aggregates can be in such a case privileged. In order to estimate the size of the NiO crystallites on the support, two models were suggested, taking into account or not the presence of a solid solution of nickel in ceria. Despite the fact that these two cases describe a very simple structure of the catalysts, they allow the determination of particles size by default and by excess. The size of NiO crystallites is estimated to be between 5 Å and 15 Å for the two compounds (Table 2), but a smaller NiO crystallite size is obtained on the ternary compound. Clearly some NiO clusters smaller than the ceria grains size coexist with larger NiO crystallites observed by XRD.

3.2. Interaction of mixed oxides with H_2

3.2.1. TGA

Up to about 100 °C, the weight loss observed in H_2 corresponds to the elimination of physisorbed water, while for temperatures higher than 150 °C a more distinct domain is observed at about the temperature of reduction of NiO (Fig. 4), with the creation of anionic vacancies by the elimination of H_2O (OH groups) [6].

$$Ni^{2+} + O^{2-} + H_2 \rightarrow Ni^0 + H_2O + \square \quad (1)$$

(with □: anionic vacancy)

In Fig. 4, the loss of weight (≈6.5 wt.%) observed in the domain of reduction of NiO is in good agreement with the Ni content of the

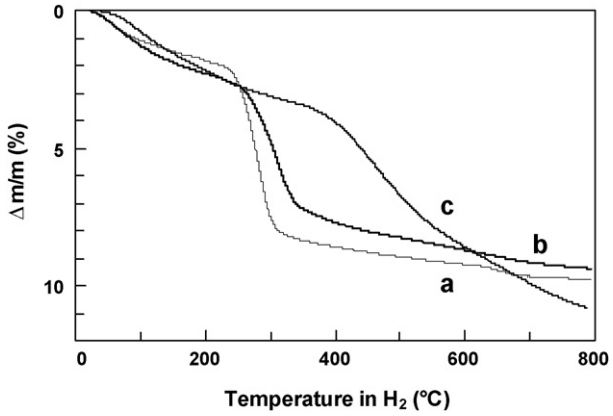

Fig. 4. Thermogravimetric profiles of (a) $CeNi_1O_Y$, (b) $CeZr_{0.5}Ni_1O_Y$ and (c) $CeAl_{0.5}Ni_1O_Y$ treated in pure H_2.

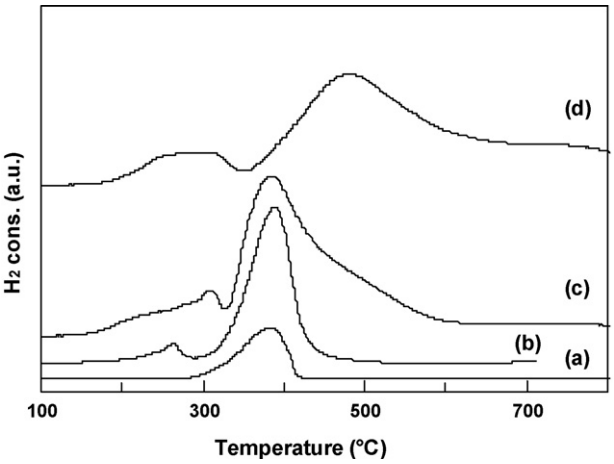

Fig. 5. TPR of (a) NiO (×0.5), (b) $CeNi_1O_Y$, (c) $CeZr_{0.5}Ni_1O_Y$ and (d) $CeAl_{0.5}Ni_1O_Y$ compounds.

solids, considering NiO is quantitatively reduced to metallic nickel according to Eq. (1) ($NiO + H_2 \rightarrow Ni^0 + H_2O$). The difference in temperature between NiO and $CeNi_XO_Y$ reduction was related to the presence of clusters or small NiO aggregates which are more easily reduced [6]. When the solid is treated for 10 h at T_T higher than 150 °C, anionic vacancies are created in higher concentration than what can be seen on classical TGA profile presented here [7].

3.2.2. TPR

The TPR profile in H_2 of NiO presents one reduction peak at about 393 °C (Fig. 5) while the mixed oxides present also a peak at lower temperature, at 275 °C on $CeNi_1O_Y$ and between 200 °C and 330 °C on ternary compounds. The second reduction peak is at the same position for $CeZr_{0.5}Ni_1O_Y$, $CeNi_1O_Y$ and NiO, while the presence of Al shifts the second peak to higher temperatures (487 °C). A linear relationship is obtained between the total hydrogen consumed during TPR with the Ni content of $CeM_{0.5}Ni_XO_Y$ and $CeNi_XO_Y$ compounds (Fig. 6), showing that H_2 is consumed in priority to reduce nickel species. The quantity of H_2 consumed in TPR analysis is in good agreement with the Ni content of the solids, as already observed with TGA experiments. The H/Ni atomic ratios obtained for the mixed oxides are slightly higher than the theoretical value of 2 necessary to reduce quantitatively NiO into Ni^0 according to Eq. (1). More specifically, H/Ni atomic ratios of about 2.3 are obtained for $CeZr_{0.5}Ni_1O_Y$ and $CeNi_1O_Y$ compounds.

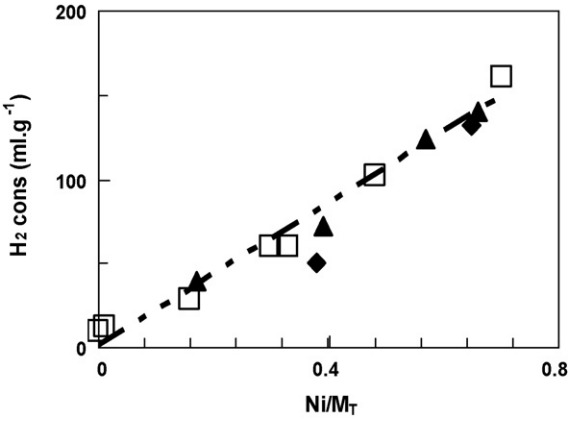

Fig. 6. H_2 consumed during TPR versus Ni content of $CeNi_XO_Y$ (□) from Ref. [11] $CeZr_{0.5}Ni_XO_Y$ (▲) and $CeAl_{0.5}Ni_XO_Y$ (◆) compounds.

A first maximum temperature reduction peak at about 264 °C was observed for low Ni contents in $CeNi_XO_Y$ solids, when the Ni^{2+} species is only present either in the solid solution of cerium–nickel or in small NiO crystallites [11]. It is usually reported that TPR analysis of CeO_2 presents two peaks at about 500 °C and 820 °C, and that the reduction peak obtained at temperature higher than 700 °C (not analyzed here) corresponds to the reduction of bulk Ce^{4+} to Ce^{3+} [12]. Moreover, it was also shown that NiO facilitates the reduction of a cerium solid solution [6]. Therefore it can be proposed that TPR peaks correspond to the reduction of nickel species in various environments. The low temperature peak can be attributed to nickel species: (i) belonging to the solid solution and/or to (ii) small NiO crystallites, easily reducible, (but with the simultaneous reoxidation of a part of these species by reduction of some Ce^{4+} ions and Zr^{4+} ions). Then the larger NiO crystallites are reduced when increasing temperature.

3.2.3. Hydrogen storage (chemical titration)

At 150 °C, in a helium + isoprene flow, alkadiene hydrogenation occurs on H_2 treated compounds. As a function of time on stream, the hydrogenation activity decreases and by integrating the curve obtained, the extractable reactive hydrogen content (H*) of the solid can be determined [10]. For all the solids studied, the extractable hydrogen content is found dependent on treatment temperature T_T in H_2, on nickel content, and on the presence of M (Figs. 7 and 8). For $T_T \geq 150$ °C, a hydrogen storage between 10×10^{-3} mol g^{-1} up to 100×10^{-3} mol g^{-1} is measured. In a wide range of temperatures T_T, interesting gravimetric hydrogen storage (4 up to 6 wt.%) and volumetric hydrogen storage (240 g l^{-1} and 300 g l^{-1}—taking into account the measured density of the solids) can be obtained. Besides, $CeZr_{0.5}Ni_1O_Y$ treated in H_2 at 200 °C allows to obtain one exceptional point with a hydrogen storage of 100×10^{-3} mol g^{-1}, i.e. 10 wt.% or 540 g l^{-1}. Ternary mixed oxides present higher hydrogen storage capacities and better stability with the temperature T_T than the binary compound (Fig. 7). Moreover, when $x = 1$ an optimum hydrogen storage is obtained. As shown in Fig. 8, $CeNi_1O_Y$ presents higher results than $CeNi_{0.5}O_Y$ and on ternary $CeM_{0.5}Ni_XO_Y$ (M = Zr or Al) compounds with X higher than 1 and up to 3, no better results were observed [7]. For comparison, NiO prepared in similar conditions was also analyzed. As for binary mixed oxides, optimum hydrogen storage is observed for a treatment temperature of 250 °C, while for higher T_T the hydrogen content decreases drastically.

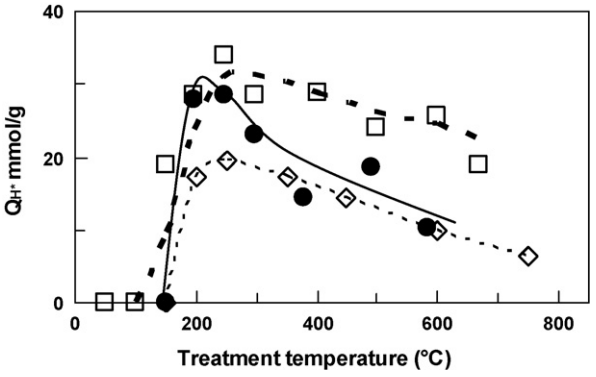

Fig. 8. H* species concentration as a function of treatment temperature T_T in H_2 of $CeNi_{0.5}O_Y$ (◇) from Ref. [8], $CeNi_1O_Y$ (□) and NiO (●) compounds.

Much higher hydrogen storage is measured with chemical titration compared to TGA and TPR analysis. For comparison, while hydrogen storage of 10 wt.% can be measured with chemical titration, only about 1 wt.% of H_2 is consumed during TPR on $CeZr_{0.5}Ni_1O_Y$. Even if through TPR, a higher than necessary H/Ni atomic ratio is obtained to reduce NiO, in agreement with an insertion of hydrogen species in the solid, the difference obtained is too high to be explained easily. However, it is important to note that TPR experiments are obtained with a progressive increase of temperature up to 800 °C in 5% H_2–95% Ar mixture while for chemical hydrogen titration the solid is activated in pure H_2 during 10 h at 200 °C.

3.2.4. INS

The H_2 treatments at 100 °C and 250 °C generate an increase of the spectrum level with T_T showing an insertion of hydrogen species into $CeAl_{0.5}Ni_1O_Y$ solid in H_2 (Fig. 9). It is important to

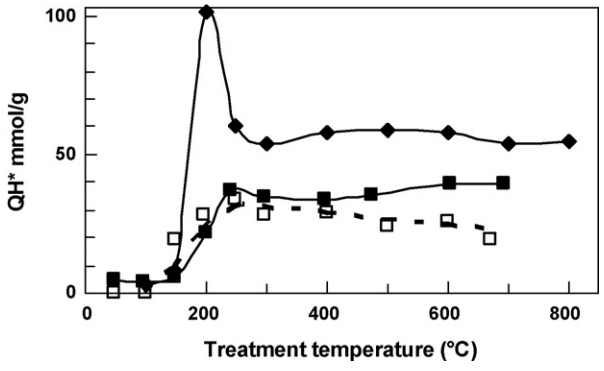

Fig. 7. H* species concentration as a function of treatment temperature T_T in H_2 of $CeZr_{0.5}Ni_1O_Y$ (◆) from Ref. [7], $CeAl_{0.5}Ni_1O_Y$ (■), and $CeNi_1O_Y$ (□) compounds.

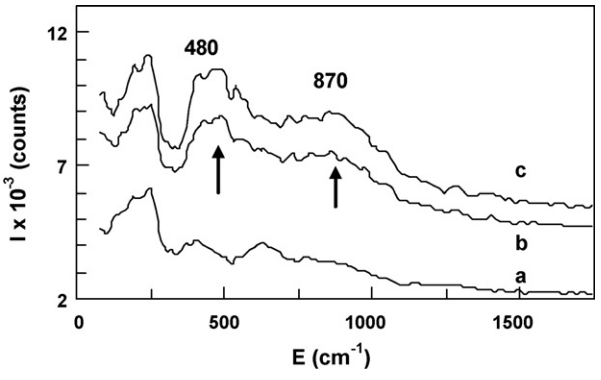

Fig. 9. INS spectra of $CeAl_{0.5}Ni_1O_Y$ treated (a) in vacuum at 200 °C, and in H_2 at (b) 100 °C and (c) 250 °C.

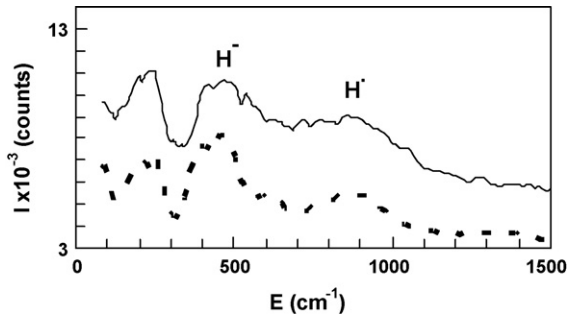

Fig. 10. INS spectra of $CeAl_{0.5}Ni_1O_Y$ and $CeNi_1O_Y$ (...) compounds treated in H_2 at 250 °C.

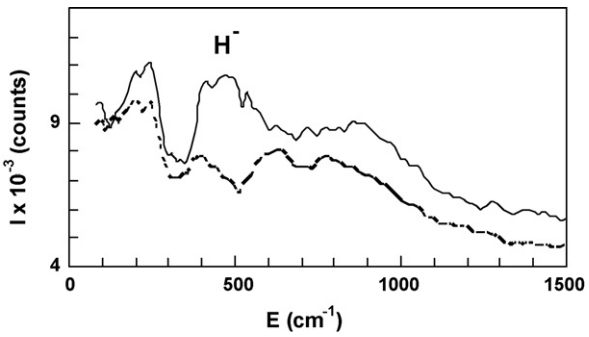

Fig. 11. INS spectra of $CeAl_{0.5}Ni_1O_Y$ treated in H_2 at 250 °C (—) followed by a treatment in O_2 (...) at ambient temperature.

remind that the spectrum level is proportional to the hydrogen content. Moreover, Fig. 10 shows that $CeAl_{0.5}Ni_1O_Y$ compound inserts a higher content of hydrogen than $CeNi_1O_Y$ solid after treatment in H_2 at 250 °C. All these results are in good agreement with those obtained by chemical titration. The INS spectrum shows some hydrogen species with vibration bands at about 250 cm^{-1}, 400 cm^{-1} and 630 cm^{-1}, assigned to OH groups already present in the solid treated in vacuum at 200 °C [13]. Besides, two intense and large bands at about 480 cm^{-1} and 870 cm^{-1} are only observed on H_2 treated solids, due to the insertion of different hydrogen species. The band at about 480 cm^{-1} can be assigned to hydride species [13,14], while the large band at about 870 cm^{-1} can be attributed to the presence of hydrogen species in interaction with metallic nickel species Ni^0 [15]. When H_2 treated solid is oxidized at ambient temperature in air, the peaks assigned to hydride species disappear (Fig. 11), meanwhile an intense large band at 630 cm^{-1} related to the formation of OH groups appears. The reaction is exothermic in agreement with a violent reactivity of hydride

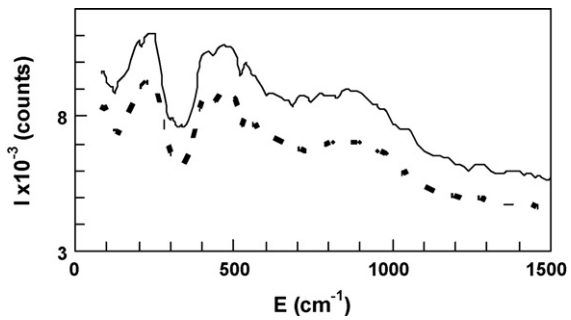

Fig. 12. INS spectra of $CeAl_{0.5}Ni_1O_Y$ treated in H_2 at 250 °C (—) and after reaction with isoprene (...): according to chemical titration about 15% of H* species are consumed.

species with oxygen. The reactivity of the hydrogen species in the catalytic reaction was also analyzed. After treatment in H_2 at 250 °C, $CeAl_{0.5}Ni_1O_Y$ was treated in isoprene (6 Torr in helium) at 150 °C (Fig. 12). The spectrum level decreases and the bands at about 250 cm^{-1}, 480 cm^{-1} and 870 cm^{-1} are affected. It can be estimated from the chemical titration that about 15% of the hydrogen species are consumed in such conditions. It appears that hydrogen species of different nature (H^-, H^+, and H) are involved in the catalytic reaction.

3.3. Discussion

Hydrogenation mechanism during catalytic reaction in H_2 was described by a nucleophilic attack of diene, with a hydride nature of the first hydrogen introduced in the molecule [16]. It was shown that three coordinatively unsaturated site (noted 3 CUS or ^{3}M) is the prerequisite condition to obtain alkadiene hydrogenation activity. Therefore, in helium + alkadiene (chemical titration), the H* species are for one half H^- species located in the anionic vacancies and the second half H^+ species coming from OH groups as presented in Scheme 1. Furthermore, on various non-metallic catalytic materials, by taking into account the structure of the solid and the existence of strong interaction between two cations, different ^{X}M–^{Y}M′ sites (where X and Y are the number of unsaturations or the number of anionic vacancies, on each M and M′ cation), were proposed to be the active sites for hydrogen storage [5]. For studied solids, the high hydrogen storage obtained can be explained by a high proportion of Ni cations in strong interaction with other cations in (i) solid solution of ceria or ceria–zirconia and (ii) small NiO crystallites (Scheme 2). The reduction of the Ni^{2+} cations facilitates the reduction of Ce^{4+} cations in their vicinity with the simultaneous reoxidation of these Ni species (Eq. (2)) [6]. This phenomenon increases the amount of anionic vacancies created. The presence of Zr^{4+} cations in the ceria–zirconia solid solution also affects the redox process as the

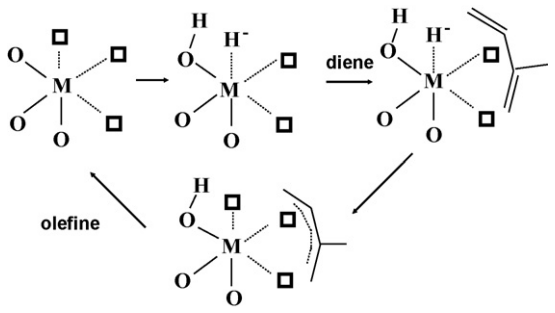

Scheme 1. Diene hydrogenation mechanism on a ^{3}M site (three anionic vacancies on M cation, □: anionic vacancy). Surface hydrogen is regenerated by bulk hydrogen.

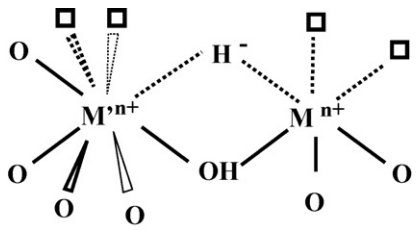

Scheme 2. Active site generated in H_2 on cerium and nickel-based mixed oxides at NiO crystallite and CeO_2 or solid solution interface [5,7]. (M^{n+} = Ni^{2+}, $Ni^{\delta+}$, M'^{n+} = Ce^{4+}, Ce^{3+}, Al^{3+}, Zr^{4+}, Zr^{3+}, Ni^{2+}, or $Ni^{\delta+}$, □: anionic vacancy–number arbitrary–).

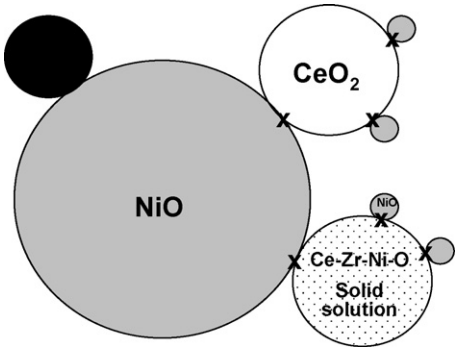

Scheme 3. Metallic Ni^0 (●), small and large crystallites of NiO (●), CeO_2 (○) or cerium (and zirconium) and nickel solid solution (⊙) interfaces (x). Ni^0 crystallite size is not known.

participation of Zr^{3+} cations has to be envisaged [17] (Eq. (3)) and explains the highest hydrogen storage for the Zr containing compound.

$$2Ce^{4+} + Ni^0 \leftrightarrow 2Ce^{3+} + Ni^{2+} \quad (2)$$

$$2Zr^{4+} + Ni^0 \leftrightarrow 2Zr^{3+} + Ni^{2+} \quad (3)$$

During the activation treatment in H_2 at T_T beside Eq. (1), the anionic vacancy is filled with hydride species by heterolytic splitting of H_2:

$$O^{2-}M^{n+}\square + H_2 \rightarrow OH^-M^{n+}H^- \quad (4)$$

The INS experiments show the presence of H^- and H^+ species but also of uncharged hydrogen species. It is well known that metallic nickel is able to adsorb hydrogen, therefore in addition to the route described above, the homolytic dissociation of H_2 on Ni^0 is also considered and these species can be titrated on a hydrogenation site by migration [6]:

$$H_2 \rightarrow 2H \quad (5)$$

Finally, hydrogen species of different nature coexist related to different phases in presence: CeO_2, NiO (small and large crystallites), solid solution, and metallic Ni, as presented in Scheme 3. One should notice that Ni^0 was not seen by XRD or XPS after treating the solid in H_2 at 200 °C (10 h) [6] and only INS experiments lead to take its presence in consideration. Moreover, hydrogen species of different nature can also be present and participate to the chemical titration, such as adsorbed H_2, unseen by INS in the studied conditions.

4. Conclusion

$CeM_{0.5}Ni_XO_Y$ (M = Zr or Al, $0 \leq X \leq 3$) mixed oxides are large catalytic hydrogen reservoirs. Different characterizations show the presence of a solid solution and/or a highly dispersed nickel oxide in ceria (or ceria–zirconia) allowing an easy reversible reducibility of the active Ni species by a redox process. Particular active sites, involving anionic vacancies and reactive hydrogen are created during the activation in H_2. Hydrogen species of different nature such as hydride species, hydrogen species in interaction with metallic nickel, as well as hydrogen species of hydroxyl groups coexist and participate, directly or by diffusion, to the chemical titration of hydrogen.

Acknowledgements

The authors thank ILL (Institut Laue Langevin, Grenoble) for supporting this work and acknowledge the help of the ILL group. SD is grateful for a MESR grant from ministry.

References

[1] J.P. Marcq, J.P. Bonnelle, M. Pinabiau, Patent FR2607131 to BP (1988).
[2] M.P. Sohier, G. Wrobel, J.P. Bonnelle, J.P. Marcq, Appl. Catal. 84 (1992) 169.
[3] Y. Barbaux, J.P. Marcq, H. Diaz, M. Pinabiau, Patent EP0208405 to BP (1987).
[4] L. Duhamel, Patent WO2004041724 to CNRS and University of Lille 1 (2004).
[5] L. Jalowiecki-Duhamel, Int. J. Hydrogen Energy 31 (2006) 191 (and references therein).
[6] C. Lamonier, A. Ponchel, A. D'Huysser, L. Jalowiecki-Duhamel, Catal. Today 50 (1999) 247 (and references therein).
[7] L. Jalowiecki-Duhamel, J. Carpentier, A. Ponchel, Int. J. Hydrogen Energy 32 (2007) 2439.
[8] L. Jalowiecki-Duhamel, A. Ponchel, C. Lamonier, Int. J. Hydrogen Energy 24 (1999) 1083.
[9] A. Ponchel, A. D'Huysser, C. Lamonier, L. Jalowiecki-Duhamel, Phys. Chem. Chem. Phys. 2 (2000) 303.
[10] L. Jalowiecki, M. Daage, J.P. Bonnelle, A. Tchen, Appl. Catal. 16 (1985) 1.
[11] L. Jalowiecki-Duhamel, H. Zarrou, A. D'Huysser, Proceedings of the IHEC 2007, Istanbul, Turkey, 2007.
[12] P. Fornasiero, R. Di Monte, G.R. Rao, J. Kaspar, S. Meriani, A. Trovarelli, M. Graziani, J. Catal. 151 (1995) 168.
[13] C. Lamonier, E. Payen, P.C.H. Mitchell, S. Parker, J. Mayers, J. Tomkinson, Stud. Surf. Sci. Catal. 130 (2000) 3161.
[14] H. Jobic, G. Glugnet, M. Lacroix, S. Yuan, C. Mirodatos, M. Breysse, J. Am. Chem. Soc. 115 (1993) 3654.
[15] F. Hochard, H. Jobic, J. Massardier, A.J. Renouprez, J. Mol. Catal. A 95 (1995) 165.
[16] L. Jalowiecki, G. Wrobel, M. Daage, J.P. Bonnelle, J. Catal. 107 (1987) 375.
[17] A. Trunschke, D.L. Hoang, H. Lieske, J. Chem. Soc. Faraday Trans. 91 (1995) 4441.